JOURNAL OF MATERIALS SCIENCE 13 (1978) 711–721

An investigation of the microstructure and mechanical properties of high density polyethylene spherulites

A. LOW*, D. VESELY*, P. ALLAN*, M. BEVIS*
Department of Metallurgy and Materials Science, University of Liverpool UK

Scanning transmission electron microscopy and related techniques have been used to characterize the micromorphologies of high-density polyethylene spherulites produced under different crystallization conditions. The experimental techniques used in the investigation are summarized, as are some relationhips between spherulite morphology, crystallization conditions and mechanical properties. A preliminary model for the micromorphology of banded polyethylene spherulites is proposed.

1. Introduction

The aim of this paper is to bring together three pieces of research which when combined demonstrate important relationships between the crystallization conditions, microstructure and mechanical properties of semicrystalline polymers. The three pieces of research are as follows: (i) The development of scanning transmission electron microscopy techniques for the study of electron beam sensitive crystalline/semicrystalline materials [1]. (ii) The detailed study of the microstructure of polyethylene spherulites produced under different crystallization conditons in bulk specimens and thin films [2]. (iii) Systematic studies of the relationships between crystallization conditions and the mechanical properties of a range of high- and low-density polyethylenes and other semicrystalline polymers [3].

The need for a better electron optical method for gaining more detailed information about the microstructure of semicrystalline plastics was realized by the authors in previous studies of deformation processes in polyethylene spherulites [4]. The detail of the information and the rate at which it could be gained by conventional transmission electron microscopy was severly limited. Of more concern to the authors was the reliance they had to place on previous models for the microstructure of spherulites in the interpretation of selected-area electron diffraction patterns.

The need for further work on the characterization of the microstructure of spherulites, which would be dependent on the development of better analytical techniques, became more urgent when it was realized that marked differences in the mechanical properties of several semicrystalline thermoplastics could be produced by systematically changing the crystallization conditions used during fabrication. The relationships between crystallization conditions, microstructure and properties are only described for the case of linear polyethylene in this paper, although tests on poly-4-methylpentene-1, poly(tetramethylene terephthalate) and low-density polyethylene also show similar trends.

2. Mechanical testing and light microscopy results

Representative load–elongation curves for two ASTM tensile bars of high-density polyethylene, HDPE 3 as supplied by the Polymer Characterization Centre, Rubber and Plastics Research Association, $\bar{M}_w = 68\,000$ $\bar{M}_n = 11\,400$, which were prepared from 3 mm thick compression-

*Present address: Department of Non-Metallic Materials, Brunel University, Uxbridge, Middlesex, UK

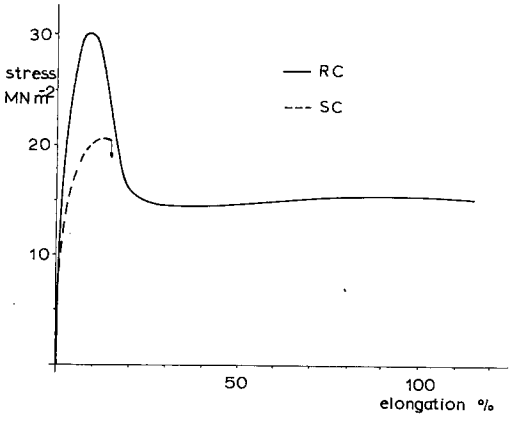

Figure 1 Load–elongation curves for two ASTM tensile bars of HDPE 3. The continuous curve corresponds to a rapidly cooled specimen (RC), tested at a cross-head speed of 50 mm min^{-1}. The broken curve corresponds to a slowly cooled specimen (SC), tested at a cross-head speed of 0.05 mm min^{-1}.

moulded plaques are shown in Fig. 1. The continuous curve represents the behaviour of specimens prepared from plaques which were quenched into water at 283 K after being held at 483 K in the compression-moulder for 10 min. The broken curve represents a much more brittle behaviour and is representative of the specimens which were cooled from 483 to 398 K and held at the latter temperature for approximately 180 min for crystallization. The cross-head speeds for the tests were 50 and 0.05 mm min^{-1} respectively for quenched and slow-cooled specimens of the same geometry.

A light microscopy study of microtomed sections of the bars produced under the two crystallization conditions showed a significant difference in microstructure. Fig. 2a shows a section which is representative of the whole of the slow-cooled specimen. Fig. 2b shows a section prepared by sledge-microtomy of the quenched specimen. In the latter there is a variation in microstructure from the edge to the centre which is related to the change in cooling rate at different positions in the plaque. The edge appears to be structureless at the magnification shown, but just below the surface some banded spherulites with a band-spacing of $\sim 1.0\,\mu m$ are visible. As the distance from the surface increases the bands in the spherulites become more widely spaced until they eventually disappear in the central region.

A straightforward fracture surface study showed that crack initiation and propagation in the rapidly cooled specimen primarily occurred from the central region and produced the type of fracture surface shown in Fig. 3a. The slow cooled specimens gave the characteristic fracture surface associated with brittle failure at a much lower cross-head speed of 0.05 mm min^{-1} as shown in Fig. 3b. The important feature of this fracture surface is the absence of any drawn polymer over the whole area which indicates that the specimen was brittle through its volume.

A similar type of behaviour has been observed in injection moulded specimens of HDPE when the mould temperature was varied from 308 to 353 K, all other processing conditions remaining constant. Microtomed sections of the specimens were taken from the centre of the injection-moulded tensile bars and an example from a bar moulded at 308 K is shown in Fig. 4. Fig. 4a is a low magnification micrograph taken in cross polars and shows the regions of differing microstructure through the thickness of the injection-moulded bar. The two broad regions which appear just below the highly

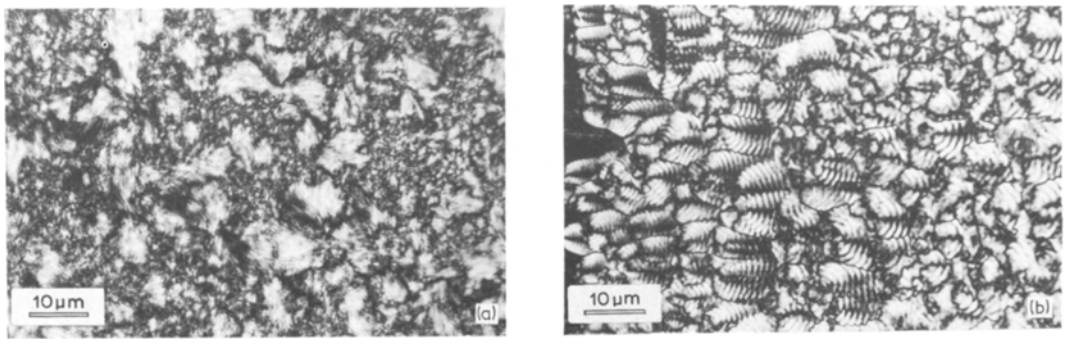

Figure 2 (a) A transmission optical micrograph, taken between crossed polars, of a microtomed section of a compression-moulded plaque of HDPE 3 which had been slowly crystallized. This structure is representative of the whole cross-section of the plaque. (b) A transmission optical micrograph of a microtomed section of a compression-moulded plaque of HDPE 3 which had been rapidly crystallized. The surface of the plaque is on the left.

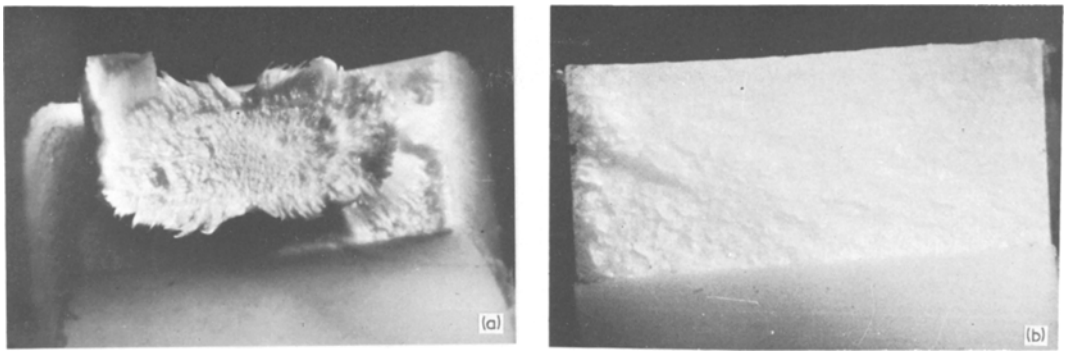

Figure 3 (a) Photograph of the fracture surface from a rapidly cooled compression-moulded specimen of HDPE 3 tested at 293 K. The cross-head speed was 750 mm min^{-1}. (b) Photograph of the fracture surface from a slowly crystallized compression-moulded specimen of HDPE 3 tested at 293 K. The cross-head speed was 0.05 mm min^{-1}.

oriented skin are composed of a banded spherulite microstructure which is accounted for by the rapid cooling of the surface. This is shown in Fig. 4b. The central band which is shown in Fig. 4c is composed of microstructures of similar size to those shown in Fig. 4b but with the notable absence of the banded contrasts. This structure is consistent with the slower cooling conditions of the central region.

The specimens moulded at 353 K show a reduction in the thickness of the banded spherulite region and an increase in the width of the central zone of the bar.

When tested at room temperature with a cross-head speed of 100 mm min^{-1} the elongations to failure of the bars prepared with mould temperatures of 308 and 353 K were 184% and 79% respectively.

Under these conditions, both types of specimen necked and the fracture processes were very similar, except for the fact that the specimens moulded at 353 K always started to fail in the central region. This is illustrated in Fig. 4d. The difference in mechanical properties of the two types of specimen can be accounted for by the effect of the moulding temperatures on their microstructures.

The results summarized above show clearly that the rate of crystallization of high-density polyethylene governs the morphology of the solid polymer, and that the nature of the micromorphology greatly influences the mechanical behaviour. Consequently, one of our main objectives was to try to determine, using light and electron microscopy techniques, the difference in micromorphology between the ductile material characterized by the banded spherulites in Fig. 2b and the brittle material characterized by the morphology shown in Fig. 2a. Previous studies have not brought out the differences in micromorphologies of the spherulites represented by the two micrographs.

Light microscopy, primarily on high-density polyethylene [5–8], led to the proposal that spherulites in this material were composed of ribbon-like lamellae radiating from a central nucleus in such a way that the [010] crystallographic direction always lay parallel to the radius. Furthermore, it was postulated that the lamellae twist periodically about the radial direction. The period of the twist was shown to decrease with increased crystallization rate is indicated by the separation of the concentric rings observed in the spherulite under polarized transmitted light [14]. Electron microscopy of the debris remaining after selective oxidation of polyethylene spherulites [12] tended to confirm the previous light microscope observations. A second model in which the light microscopy observations were explained by a variation in chain-axis orientation of the lamellae along the spherulite radius has also been proposed [15, 16] but no further experimental evidence for this theory has been produced. Electron microscopy studies of polyethylene spherulites [9–13] have been on either thin films or bulk samples of polyethylene, using conventional electron microscopy and scanning electron microscopy respectively. The transmission electron microscopy of ultra-thin sections of bulk polyethylene [13] led to the proposition that the banded spherulites of poly-

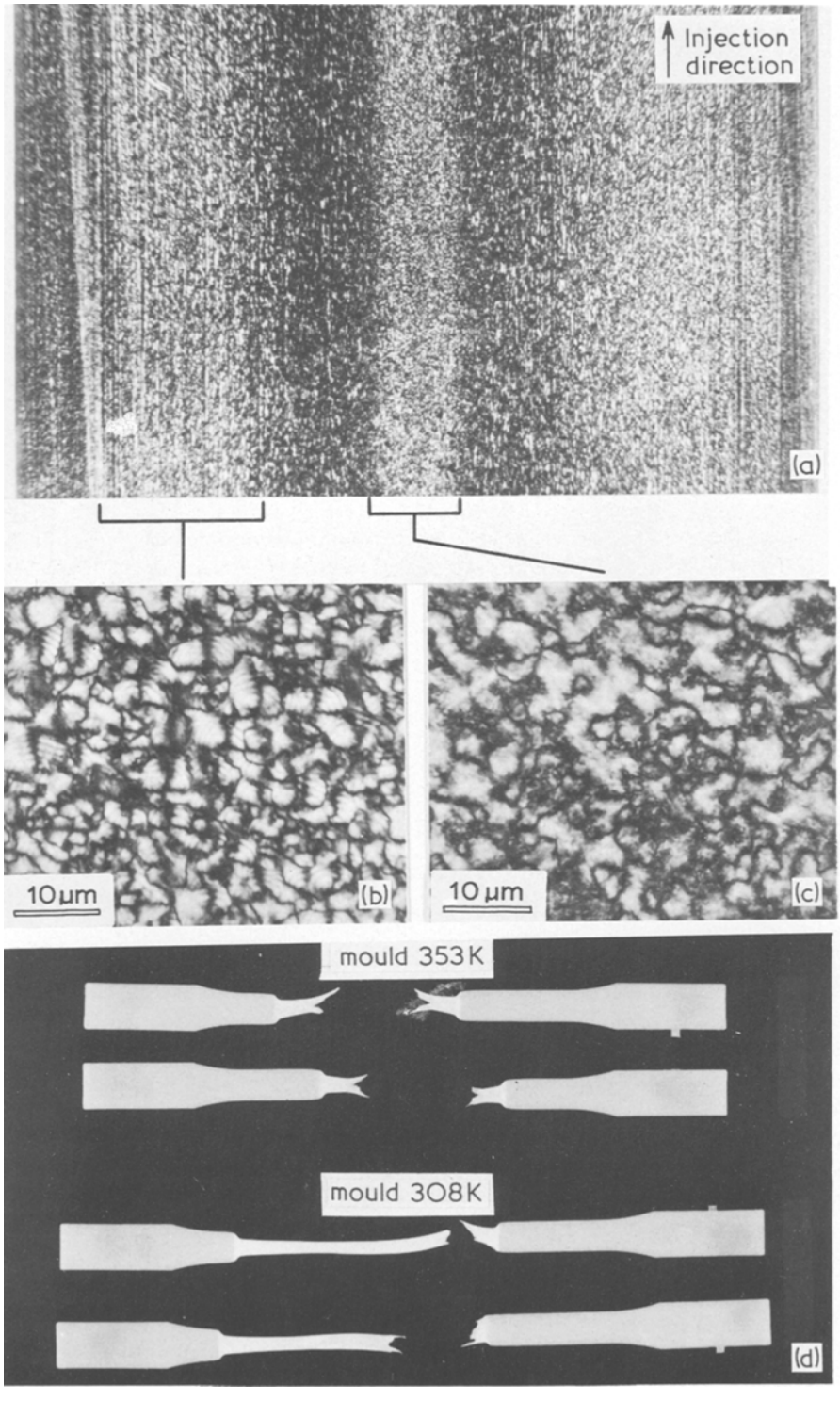

Figure 4 (a) Low magnification optical micrograph taken between crossed polars of a microtomed section of an injection-moulded tensile bar of HDPE 3. The temperature of the mould was 308 K. The regions of differing microstructure are clearly visible. (b) Transmission optical micrograph taken between crossed polars of one of the two broad regions of the section shown in Fig. 4a which contains a banded spherulite microstructure. (c) Transmission optical micrograph taken between crossed polars of the central region of the section shown in Fig. 4a. (d) Injection-moulded specimens of HDPE 3 after being tensile tested at 293 K with a cross-head speed of 100 mm min^{-1}. The specimens moulded at 308 K have more than twice the elongation to failure of those moulded at 353 K.

ethylene were composed of regions of varying crystallinity, but no details on the microstructure of these regions could be resolved.

The main limitation on the use of electron microscopy techniques is that the electron beam interacts with the polymer and causes structural changes within the specimen while under observation. In fact, recent experiments on spherulites of polyethylene have tried to exploit the effects of radiation on the polymer in attempts to obtain information about the original structure [10, 11]. Very few workers, however, have used electron diffraction to obtain detailed information of the microstructure of polyethylene spherulites. The main reason for this has been the problem of the detrimental effect of electron radiation on the crystalline regions of the specimens. Early work by Keller and Sawada [12] used electron diffraction information from polyethylene spherulite debris which had been produced by selective oxidation with fuming nitric acid. More recently electron diffraction has been used to characterize the deformation in high-density polyethylene spherulites [4]. Neither of these studies, however, provided information from undamaged spherulites which would give a comprehensive explanation of their micromorphology.

3. Electron microscopy

It is clear from the results summarized in Section 2 that a detailed knowledge of micromorphology of the two types of spherulite is needed if the reasons for the difference in the behaviour of rapidly and slowly cooled high-density polyethylene is to be understood. Electron microscopy is clearly the technique that has to be used to reveal structural features on a very fine scale. However, most synthetic polymers are very sensitive to electron beam damage and it is difficult to obtain reliable information from undamaged specimens. To overcome this difficulty we recently adopted the scanning transmission electron microscopy (STEM) technique for studying semicrystalline polymers and have developed the operating conditions which enable us to obtain bright-field images, microdiffraction and dark-field images from a particular diffraction spot with minimum or no further adjustment of the microscope. This is particularly important when detailed information from one area of a beam-sensitive material is needed, such as different dark-field images or sequences of diffraction patterns from closely spaced regions. The unique design features of the objective lens of the JEOL electron microscopes enabled us to gain the required information easily, all observations reported here were gained using a JEOL JEM 200B electron microscope.

The major advantage of STEM over other techniques for this particular application is in its efficient use of electrons. For example, fast-scanning can be used for focusing and selection of the area to be studied in detail; only the area observed is irradiated in both imaging and diffraction modes, and the brightness and contrast of the image can be enhanced electronically. To ensure that most of the electrons are utilized in image formation and in order to obtain dark-field from a single diffraction spot, it is essential to match the illuminating angle and the dimensions of the contrast aperture, and further to descan the beam, so that only the minimum number of electrons are lost on the contrast aperture. This is achieved by a suitable combination of objective and condensor lens currents and by changing the specimen height in the objective lens pole-piece [1].

Using this technique the beam damage was controlled to such a level that 20 bright- or dark-field images could be recorded at a magnification of ~ 5000 times (5 images at 15 000 times) from a polyethylene thin film. Another advantage of the STEM technique is the microdiffraction mode, in which the beam can be very coherent and simultaneously of a small diameter. The size of the selected diffraction area is then given by the beam diameter and can vary from several μm to 0.02 μm, depending on a combination of the condensor and objective lens currents. The lower limit of the beam diameter is given by a compromise between the life time of the specimen and the exposure time of the film, e.g. for a fast film (Kodirex) it is typically 0.1 μm for polyethylene. The diameter of the beam has been measured by the profile of the line scan across the edge of a specimen and checked by measuring the size of the contamination marks. The deflection of the beam on the cathode ray tube of the STEM display system and the electron beam on the specimen are synchronized for both the stationary and the scanning mode. Therefore the position of the beam on the tube could be related to both the recorded image and the diffraction area of the specimen. Because the beam damage is confined to the selected area without

affecting the neighbouring regions, systematic studies of local changes of crystallographic orientations are possible.

3.1. Specimen preparation

The specimens used in this work were prepared by solvent-casting and melt-casting. Following extensive investigations [2, 3] two distinct types of spherulites were chosen for detailed examination, and they are represented by the spherulites shown in Fig. 5a and b. These morphologies have been shown to be representative of the bulk material and the spherulitic films were prepared in the following ways: (a) The slowly crystallized films, represented by Fig. 5a and exhibiting spherulites which will be referred to as S (slowly crystallized) type, were solvent-cast onto a substrate and subsequently melted at 453 K and then crystallized at between 393 and 403 K for 30 min in a vacuum. (b) The rapidly crystallized films, represented by Fig. 5b and exhibiting spherulites which will be referred to as R (rapidly crystallized) type, were cast from boiling solution of polymer in solvent onto a liquid substrate of glycerol at 383 K, and as soon as evaporation of the solvent was complete the film was cooled to room temperature. The thickness of these specimens was typically 300 to 700 nm as estimated from the relative positions of contamination marks on upper and lower surfaces of specimens which were rotated after irradiation in the electron microscope.

3.2. STEM results

3.2.1. Bright-field images

The basic differences between the two types of film are clearly visible in bright-field images. The rapidly crystallized films consist of well-developed R type spherulites with distinct boundaries and typical banded morphology. At high magnifications, as shown in Fig. 10a a network of lines is evident with the predominant orientation of the lines being parallel to the spherulite radius.

The slowly crystallized films do not exhibit well-defined boundaries between the segments which constitute the S type spherulites. The segments rarely exhibit an angular spread in radii of greater than 90°, and the bands which are characteristic of R type spherulites are not present. At high magnifications the dark thin lines in S type spherulites are less pronounced than those observed in the R type, but there is a propensity of small dark spots which represent small diffracting regions, (see Fig. 12a).

3.2.2. Microdiffraction

The diffraction patterns taken from the R and S types of spherulites exhibit different features, although the preferred orientation of the [0 2 0] direction was approximately parallel to the spherulites for both types of spherulite. When the electron probe or selected diffraction area which is used for forming the electron diffraction patterns is large, as for example in the 3 μm case of Figs. 6a and 7a, the diffraction patterns are formed from crystallites of different orientations, resulting in an overlapping of diffraction patterns and the formation of extensive arcs. The arcs are continuous for the R type, Fig. 6a and discontinuous for the S type as shown in Fig. 7a. This effect is even more pronounced for small probe sizes as shown in Figs. 6c and 7c, where a probe diameter of 0.3 μm was used, and indicates that the misorientation of the

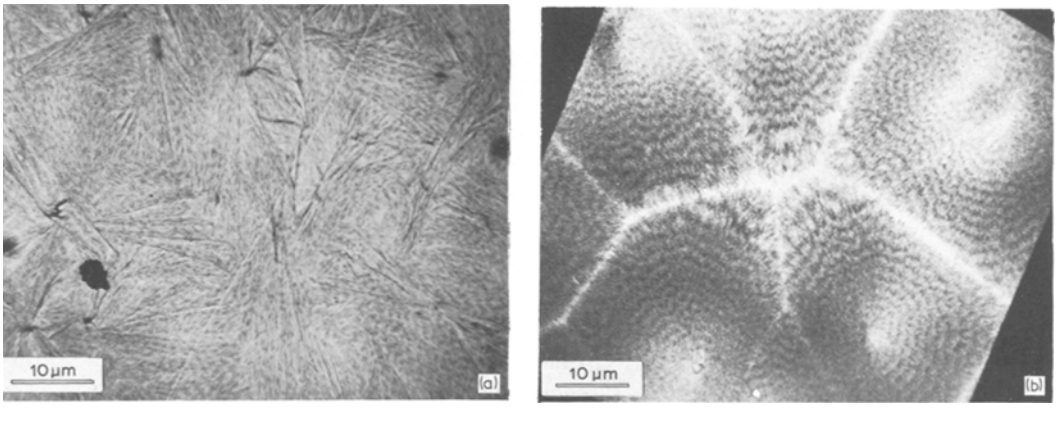

Figure 5 (a) A bright-field scanning transmission electron micrograph of a slowly crystallized film of HDPE 3. (b) A bright-field scanning transmission electron micrograph of a rapidly crystallized film of HDPE 3.

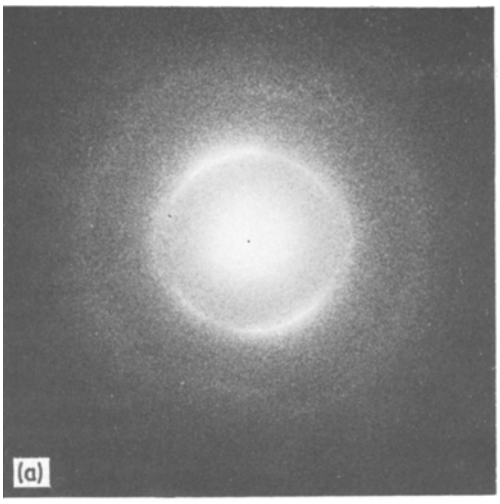

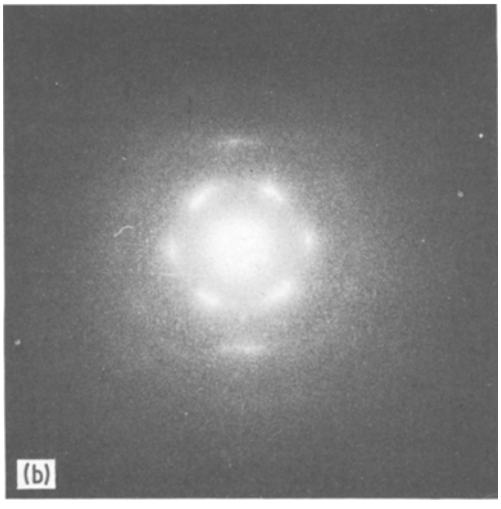

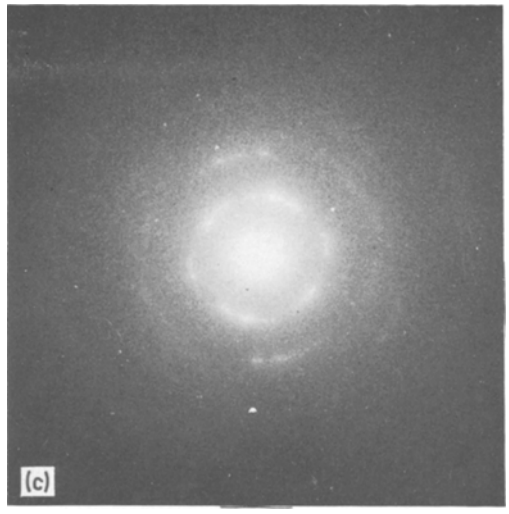

Figure 6 (a) A microdiffraction pattern from a spherulite in an R type thin film of HDPE. The pattern was taken using a 3 μm diameter probe. (b) A microdiffraction pattern from a dark band of a spherulite in an R type thin film of HDPE. This pattern was taken using a 0.3 μm diameter probe. (c) A microdiffraction pattern from a bright band of a spherulite in an R type thin film of HDPE 3. The pattern was taken using a 0.3 μm diameter probe.

crystallites or their sizes are different for the two types of spherulites.

Another important difference between the R and S type spherulties is the difference in intensities of the 1 1 0 and 0 2 0 reflections. The R type spherulites give rise to diffraction patterns which exhibit strong 1 1 0 reflections, all higher order reflections being weaker in intensity, as illustrated in Fig. 6a. In addition one set of the 1 1 0 reflections was often stronger than the other set of 1 1 0 reflections. The electron diffraction patterns from the S type spherulites, on the other hand, exhibit strong 0 2 0 reflections, which together with the other less intense reflections, represent the type of pattern used extensively by the authors in studies of the deformation processes in polyethylene spherulites [4]. Typical electron diffraction patterns from the spherulitic films shown in Fig. 5a are represented by Figs. 7a and b for thick and thin films respectively. The diffraction patterns become less complex with decreasing probe size, Fig. 7c, and can be interpreted simply in terms of a reduction in the number of low index zone axes which are parallel to the electron beam. The electron diffraction patterns can be indexed easily by making reference to Fig. 8, which is discussed in detail in a previous paper [4].

When the electron probe size which is used for forming the electron diffraction patterns is reduced to 0.3 μm, the selected area diffraction patterns obtained from bright and dark bands were different. The 0.3 μm selected area was the smallest for polyethylene which gave rise to a useful recordable diffraction pattern on high-speed film. The electron diffraction patterns obtained from the dark bands shown in Fig. 6b consist of sharp spots where the 1 1 0 reflections were more intense than all other reflections, including the 0 2 0 reflections. The reflections in the electron diffraction patterns obtained from the light bands were more diffuse and less intense than those observed in the patterns obtained from dark bands. A typical example of the former type of pattern is shown in Fig. 6c. The diffraction pattern is very similar to the large diameter selected-area pattern

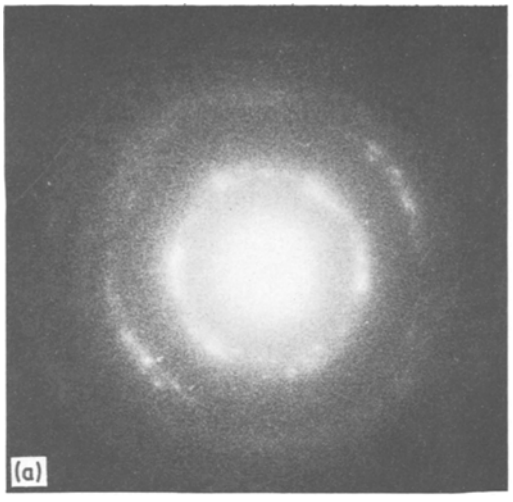

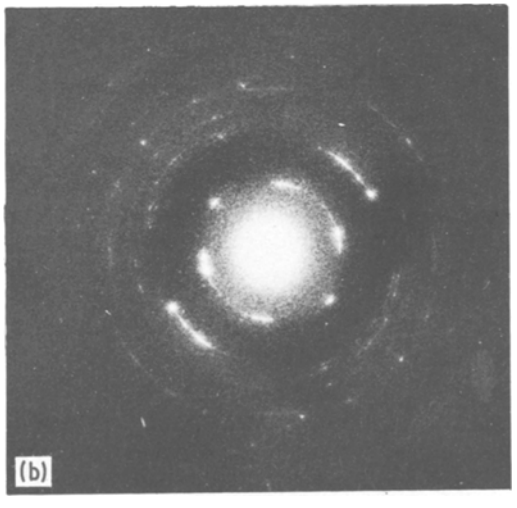

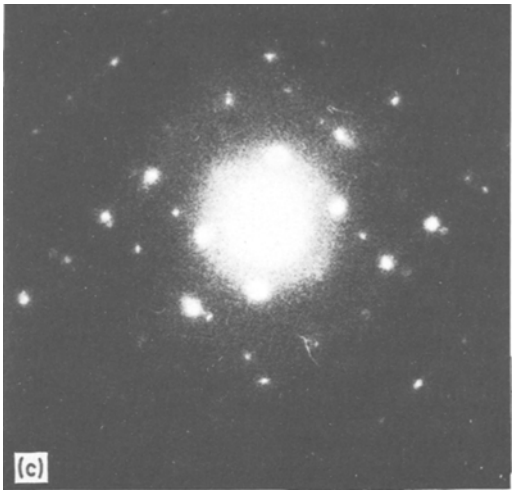

Figure 7 (a) and (b). Microdiffraction patterns from spherulites in S type thin films of HDPE 3. The patterns were taken using a 3 μm diameter probe. The films were estimated to be 0.7 and 0.3 μm thick for figures (a) and (b) respectively. (c) Microdiffraction pattern from a spherulite in an S type thin film of HDPE 3. The pattern was taken from a 0.3 μm diameter probe.

from an S type spherulite, as shown in Fig. 7a. To date the results obtained from the large selected-area electron diffraction studies can be interpreted using the model for spherulite morphology represented by Fig. 9. However this model is not supported by the interpretation of sequences of small selected area electron diffraction patterns from areas less in diameter than the band width of the R type spherulites and taken from along the spherulite radii.* There is no systematic change in the angular distribution of zone-axes with position along spherulite radii in either R or S spherulites. In our opinion, the banded diffraction contrast in the R type spherulites of the kind investigated in this work must be due to factors other than periodic twisting of lamellae.

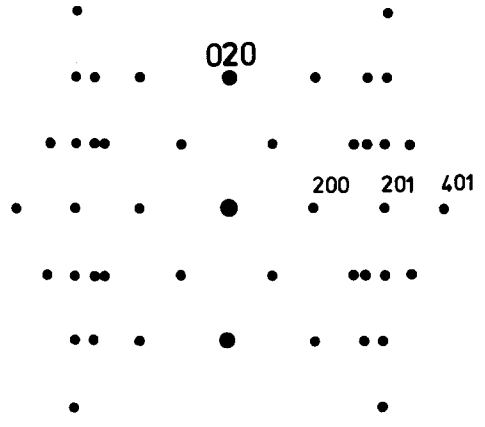

Figure 8 A construction of the electron diffraction pattern which is produced by an S type thin film of HDPE 3 when the selected area is of the order of 5 μm^2. This pattern is composed of six individual single crystal patterns which share the common 020 reflection (see [4]).

3.2.3. Dark-field images

The STEM dark-field images reflect exactly the crystallographic properties which are represented by the electron-diffraction patterns. The intensities of the reflections used in dark-field imaging can be related to the sizes of diffracting areas observed in the images. The dark-field images from the rapidly

*The interpretation of electron diffraction patterns in [4] was not dependent on a twisted-lamellae morphology in polyethylene spherulites, but simply on the existence of a range of crystal orientations with [020] parallel to the spherulite radii, which is of course represented by the diffraction patterns shown in Figs. 7a and b and Fig. 8.

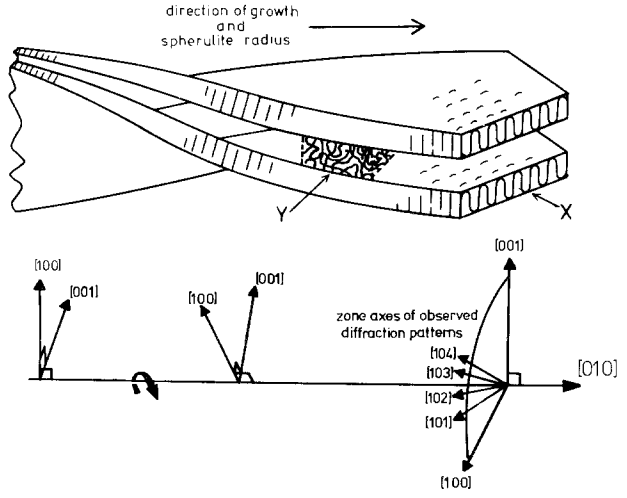

Figure 9 Schematic representation of the twisted lamellae model for the morphology of a polyethylene spherulite, showing the regularly folded (X) and interlamellar (Y) chain, and the variation in crystal axis orientations with position along a spherulite radius.

crystallized R type spherulites were very weak, other than for the 110 image arising from the stronger set of 110 reflections. In these images a very fine structure is visible at high magnification as illustrated in Fig. 10b. The density of these elongated regions varies in a periodic manner from the centre of the spherulite forming a concentric banded morphology. The contrast in dark-field images for other reflections is very weak.

The slowly crystallized S type spherulites give rise to different dark-field images which are consistent with the selected-area electron-diffraction patterns obtained fron these spherulites. In the 110/200 dark-field images only a few bright spots are observed as shown in Figs. 11b spots which correspond exactly to some of the dark spots visible in the bright-field image (Fig. 11a), the majority of dark spots in bright-field being associated with the 020 reflection. In the 020 dark-field image whole segments reflect strongly as shown in Figs. 11c and d. Similar images can be obtained for all segments as long as the 020 reflection which is approximately parallel to the spherulite radius contained within the segment is used for dark-field imaging. A comparison of 020 dark-field images for many segments shows that some segments overlap and some have common boundaries. A fine structure is visible at high magnifications, as shown in Fig. 12b and the reflecting regions probably correspond to individual lamellae of closely similar dimensions.

4. Discussion

The results presented above show that the two distinct R and S types of spherulite have a complex microstructure that can hardly be described by the models which have been proposed previously. It appears that both types of spherulite tend to grow in a direction normal to the predominant (020) planes in the crystalline phase, but the rapidly crystallized spherulites exhibit dark bands in bright-field images which are partially composed

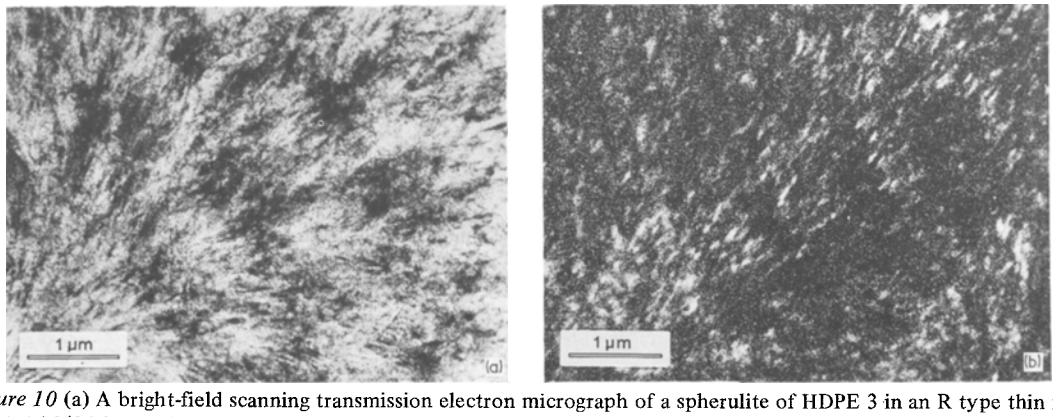

Figure 10 (a) A bright-field scanning transmission electron micrograph of a spherulite of HDPE 3 in an R type thin film. (b) A 110/200 dark-field scanning transmission electron micrograph of an R type thin film of HDPE 3.

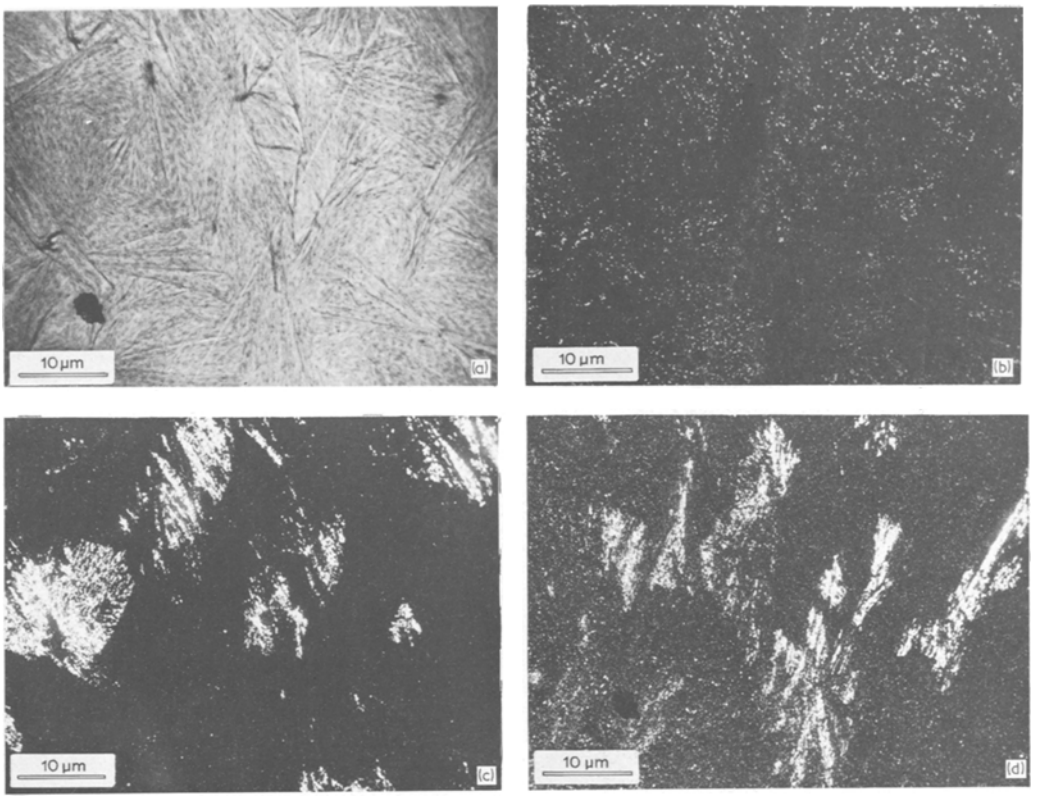

Figure 11 (a) A bright-field scanning transmission electron micrograph of a slowly crystallized film of HDPE 3. (b) A 110/200 dark-field scanning electron micrograph of the region of the film shown in (a). (c) An 020 dark-field scanning transmission electron micrograph of the region of the film shown in (a). (d) An 020 dark-field scanning transmission electron micrograph of the region shown in (a). The bright sectors in this figure have their [020] direction oriented 60° to those shown in (c).

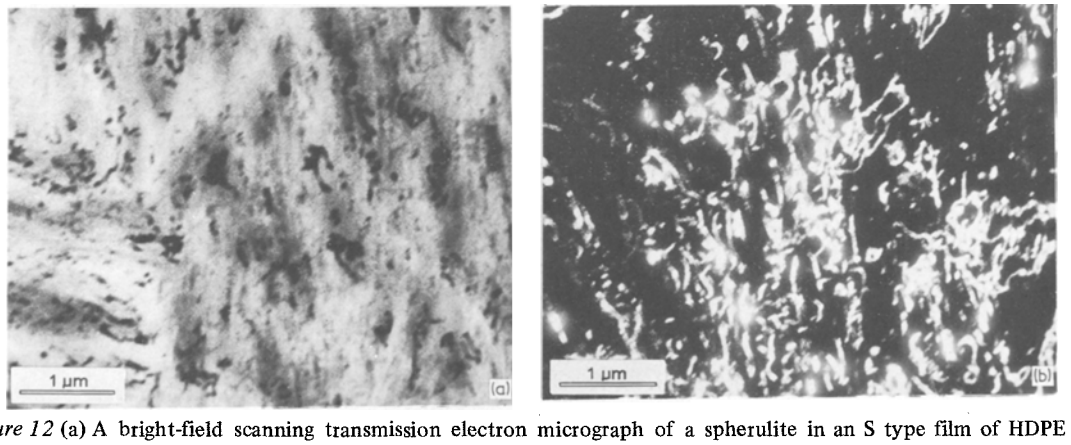

Figure 12 (a) A bright-field scanning transmission electron micrograph of a spherulite in an S type film of HDPE 3. (b) A 020 dark-field scanning transmission electron micrograph of approximately the same area shown in (a).

of crystallites which tend to grow in a direction normal to a {110} plane. Extensive investigations of the microstructures of the spherulites identified above, as well as spherulites in bulk specimens and thin films in other polyethylenes and prepared under a range of crystallization conditions, are in progress. However, at this stage sufficient work has been done to strongly indicate that in addition to small platelets there also exists a large proportion of crystalline material in the form of long fibres with a uniform diameter of about 100 nm. The difference in the distribution and crystallographic characteristics of these fibres based on our initial investigations is shown schematically in

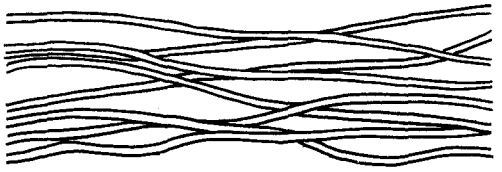

Figure 13 Schematic diagram of the arrangement of fibrils in an S type spherulite of polyethylene.

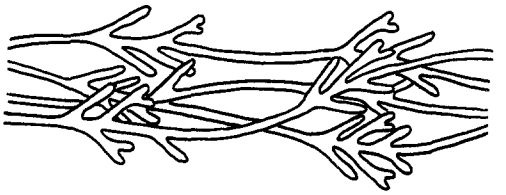

Figure 14 Schematic diagram of the arrangement of fibrils in an R type spherulite of polyethylene.

Fig. 13. The fibres tend to grow parallel to the predominant [020] direction which is approximately parallel to the spherulite radius, other than for those fibres in the dark bands in the R type spherulites which tend to grow normal to one set of {110} planes.

The orientation of the crystallites about the predominant-growth direction does vary, but not in the systematic manner represented by Fig. 9. Our results also indicate that the banded contrast observed in the R type spherulites is not determined by systematic variations in the orientation of lamellae, but by the formation of an additional type of fibre and a change in crystallinity and concentration of defects.

The formation of crystalline fibres with a growth direction parallel to [020] and with constant diameters of about 100 nm, as indicated in Fig. 14 is not consistent with previous growth models based on multiple {110} growth faces [17]. The preference for growth in the (020) planes under conditions of slow crystallization and for growth on {110} planes during rapid crystallization may be related to the transition in growth planes observed in single crystals, where with decreasing rate of crystallization the growth plane changes from {110} to (200) [18]. The relationship which is tenuous is in the tendency for the growth plane to become less closely spaced with increasing rate of crystallization.

The STEM technique [1] referred to above is now in routine use, and as stated, has been applied to the study of polyethylene spherulites. The observations on spherulites reported are however preliminary in that they are based on studies of several spherulitic films of the R and S types. Definite results in the type of work reported can only result from the examination of a large number of spherulites; work which is now in progress.

The reported relationship between mechanical properties, spherulite type and crystallization conditions is definite. The informed use of these relationships [3] should lead to an improvement in the mechanical properties of semicrystalline thermoplastic components by control of their microstructure.

References

1. D. VESELY, to be published.
2. A. LOW, D. VESELY, P. ALLAN and M. BEVIS, work in progress.
3. P. ALLAN and A. LOW, to be published.
4. P. ALLAN and M. BEVIS, *Phil. Mag.* **39** (1977) 409.
5. A. KELLER, *J. Polymer Sci.* **17** (1955) 291.
6. F. P. PRICE, *ibid* **37** (1959) 71.
7. H. D. KEITH and F. J. PADDEN, *ibid* **39** (1959) 101.
8. A. KELLER, *ibid* **39** (1959) 151.
9. J. DLUGOSZ and A. KELLER, *J. Appl. Phys.* **39** (1968) 5776.
10. D. T. GRUBB and A. KELLER, *J. Mater. Sci.* 7 (1972) 822.
11. J. E. BREEDON, J. F. JACKSON, M. J. MARCINKOWSKI and M. E. TAYLOR, *J. Mater. Sci.* 8 (1973) 1071.
12. A. KELLER and S. SAWADA, *Makromol. Chem.* **74** (1964) 190.
13. E. H. ANDREWS, M. W. BENNETT and A. MARKHAM, *J. Polymer Sci. A-2*, **5** (1967) 1235.
14. H. D. KEITH and F. J. PADDEN, *J. Polymer Sci.* **31** (1958) 445.
15. G. SCHUUR, *ibid* **11** (1953) 385.
16. *Idem, ibid* **50** (1961) 191.
17. J. J. BURNS, *J. Polymer Sci. A-2*, 7 (1969) 593.
18. T. KAWAI and A. KELLER, *Phil. Mag.* **11** (1965) 1165.

Received 15 April and accepted 19 May 1977.